



HYDROMECHANICS FOR CRYSTAL GROWTH FROM WATER-SALT SOLUTIONS

N.A. Verezub, A.I. Prostomolotov

Ishlinsky Institute for Problems in Mechanics RAS, Moscow, Russian Federation

This paper presents an overview of the current state of technological problem solving related to controlling of hydrodynamics and mass transfer in crystallizers of complex design (continuous-flowing and non-flowing) during the growth of crystals with technologically important properties (potassium dihydrogen phosphate – KDP and a mixed crystal of nickel and cobalt – KCNSH) from special water–salt solutions. Unlike crystallizers of standard designs for crystal growth from a melt (by Czochralski, Bridgman, etc.), there are also crystallizers of different design for crystal growth from water–salt solutions. According to the designers, the necessary crystal growth conditions are maintained in these crystallizers by creating the best characteristics of the flow, i.e., by controlling its velocity and direction, as well saline saturation solution and temperature. In this work, hydromechanical problems are solved for continuous-flowing and non-flowing crystallizers. The flow visualization through its physical model reveals a multi-vortex and unsteady flow structure due to mixer action, three-dimensional solution inflow and outflow and spatial crystal placement. For this reason, primary attention is given to the studies devoted to the development and application of the mathematical models for hydromechanics and heat and mass transfer based on the complete Navier–Stokes equations in the Boussinesq’s approximation for laminar regimes, as well as to the standard ($k-\varepsilon$)-turbulence model for turbulent regimes. The hydromechanical features associated with the three-dimensional flow complexity are discussed for continuous-flow crystallizers. The possibilities of maintaining the required saline saturation near the growing crystal over a long period of time are analyzed for non-flowing crystallizers. Mathematical models of convective mass transfer are considered in a "solution–crystal" conjugate formulation. The local features of hydrodynamics and mass transfer conditions in solution (saline solution saturation near growing crystal) are analyzed.

Key words: crystal growth, water–salt solution, supersaturation, hydromechanics, crystallizer, potassium dihydrogen phosphate, mixed crystal

1. Introduction

The article is devoted to a solution of technological questions of control of hydrodynamics and mass transfer in complex construction crystallizers, which are applied for growing commercially valuable crystals in special water–salt solutions: potassium dihydrogen phosphate — KDP (KH_2PO_4) and a mixed crystal of nickel and cobalt — KCNSH ($\text{K}_2\text{Ni}_x\text{Co}_{(1-x)}(\text{SO}_4)_2 \cdot 6\text{H}_2\text{O}$). These crystals are used as optical elements in nonlinear and solar-blind optics.

The KDP crystals are most spread in laser optics, where they are used as a material for various radiation frequency converters, electro-optical modulators, and phase selectors. The KDP crystals are the materials for high power laser systems, too.

The technical significance of KCNSH crystals is determined by their high transparency in “solar-blind” spectral region of ultraviolet wavelength range of 200–300 nm and almost complete opacity in other wavelength ranges. As a result, the instruments that detect a radiation in this spectrum range are capable for operating in sunlight. Such zone filtering allows maintaining high signal-to-noise ratios and achieving significant gains in ultraviolet range.

Preliminarily, it should be noted that if for the widely used crystal growth methods from a melt (Czochralski, Bridgman, zone melting and others) generally the same type of crystallizers is used, then such uniformity is not characteristic for crystal growth from a solution. There is a continuous search for new and more efficient crystallizer designs for concrete crystal kind and size. Difficulties in solving hydromechanics problems for crystal growth from a solution are generated by complex crystallizer designs. During them creating, it should be taken into account of their three-dimensional shape. Until recently, mathematical hydromechanics modeling in such crystallizers was problematic due to the lack of sufficient computer resources and appropriate software. In practice the problem was aggravated, because crystals are often growing from a solution involved in turbulent flow due to various mixing devices, itself crystal rotation, high-speed solution inflow to the crystallizer, and others.

The traditional way for increasing a crystal growth rate consist in using a forced convection for acceleration of mass transfer in a solution. The method of reversal crystal rotation is usually used. In this case, a convection may increase a crystal growth rate, but also enhance a morphological instability of crystal surface, i.e., worsen its quality.

It should be noted that a crystal growth is layered. At the face edges, the layers may be incomplete, the faces grow by small steps and generally have a stepped appearance. The kinetics of crystal growth is determined by a solution flow rate influence on its salt supersaturation of the face and by a dependence of a tangential velocity of growth steps on this supersaturation [1]. In the presence of a “dead” zone on the kinetic curve, there is a region of supersaturation, where this dependence is a nonlinear, sharply changing function. Such a region of supersaturation is undesirable from the point of view of defect formation (macrosteps and solution inclusions). The inhomogeneous distribution of supersaturation along the face leads to fluctuations in the speed of steps and morphological instability of the surface. A number of experimental [2–5] and theoretical [6, 7] studies have been carried out to determine an influence of convection on the instability of facet growth and possible imperfections. It is shown that the direction of solution flow near the solution/crystal interface has a significant effect on the occurrence of morphological instability. If the flow is directed against the movement of growth steps, then the morphological stability of the facet is preserved. On the contrary, the solution flow in direction of movement of the steps becomes the cause of its instability.

It follows from the literature analysis that a convection in solution weakens the inclusions formation and makes it possible to increase a growth rate without deteriorating the crystal quality [8]. It was found in [9] that the morphological stability can be increased by means of a reverse flow. However, its surface is not completely flowed around during a reversely rotating crystal and significant morphologically unstable areas remain. It was shown in [10] that by changing the crystal orientation, it is possible to influence on the flow near its surface and eliminate undesirable areas of low supersaturations. It was found that changing the characteristics of the flow near the crystal surface by controlling its orientation can eliminate low supersaturation regions on the crystal surface and limit the formation of inclusions. It is suggested that there is a relationship between the distribution of supersaturation on the surface and the formation of inclusions. Therefore, the regions with a low degree of supersaturation and with the presence of inclusions have the same location in the experiments.

In view of the fact that it is difficult to find experimentally the distribution of surface supersaturation, an important role is assigned to mathematical modeling of hydromechanics in solution. An important problem in mathematical description of crystal growth from a solution is an adequate matching of hydromechanical macromodel data (in continuous medium approximation) with thermodynamic micromodel data, which depicting the crystal faces growth. The work [11] is devoted for solution of this problem. In this work a significant discrepancy is discussed in the estimates of diffusion rates on crystallization surface for laminar and turbulent hydrodynamics models, which were made on the basis of analytical solutions in a particular simplified case—for a flow in a smooth pipe at high Reynolds numbers. The conjugation is carried out in terms of turbulent diffusion coefficients for a buffer turbulent boundary layer, which leads to a more acceptable (for a thermodynamic micromodel) distribution of solute concentration near growing interface in compared to traditional laminar flow approximations.

Estimates in [11] show that, in this case, salt diffusion through the turbulent boundary layer occurs much faster than through a conventional laminar layer, which can explain the more significant diffusion effect on morphological stability of crystallization surface. It is believed that a decrease of diffusion boundary layer thickness, through which perturbations can affect each other, contributes to an increase of growth surface stability [2, 6, 7]. Using the example of the KDP crystal growing, the authors of [11] discuss the experimental data connecting with a suppression of stepped groups formation on (101) face by turbulent flow, which flowing parallel to this face at velocity of 1.55 m/s. The formulas for turbulent flows from [11] are verified in studies, which use mathematical modeling of three-dimensional hydromechanics for functioning crystallizers with an experimental crystal growth rate comparison. In this case, discrepancies are fixed, which may be due to the fact that at high hydrodynamic flow rates, the crystallization rate depends only on growth kinetics, and the diffusion mode does not affect on growth rate [12, 13].

For the mixed KCNSH crystal growing, a specific problem is relevant, which is associated with an inhomogeneity of solution composition and growing crystal. In multicomponent crystals, high internal stresses are observed, leading to crack formation under mechanical stress. A technological solution to these problems can be achieved by ensuring the temperature constancy and supersaturation, the growth of only one face during crystallization, and feeding the solution according to a specially calculated law for compensation of composition crystal variations on an initial transition region [14, 15]. It is necessary to take into account of experimental data on such specific defects as mosaic microinhomogeneity and radial inhomogeneity [16, 17].

During mixed crystals growing the fluctuations of solution composition (for example, due to nonstationary convection) cause local manifestations of the isomorphic substitution reactions—complex multidirectional processes of simultaneous dissolution of a crystal and growth of a crystalline phase with different structures [18], such that the crystal surface becomes similar to a mosaic of randomly scattered zones of different composition. The isomorphic substitution reaction can be suppressed by creating some critical supercooling in the system [19], but its

effect on the mosaic pattern of microheterogeneity has not been studied. Until now, the formulation of hydromechanical problems for solving the problem of mosaic formation is very relevant for a number of reasons, for example, due to an inhomogeneity of diffusion mass transfer of various components on crystallization surface, causing different growth rates of its sections with the formation of microroughness on it.

This article summarizes the achievements in solving the problems of hydromechanics listed above for crystal growing crystals from water–salt solutions, published partially by the authors in recent years [20–23]. Specific problem statements for each crystallizer (equations and boundary conditions) are set out in the indicated articles. Crystallizers are considered, in which the solution is continuously pumped at a given temperature and the corresponding levels of salt supersaturation. Features of hydromechanics are characterized by three-dimensionality of the container and tubes for solution inflow and outflow, the complex geometry of growing crystal and its position in solution volume, the presence of rotating or vibrating devices for intensifying mixing. In addition, for the first time, the generalization includes the results for original non-flowing crystallizers, where the solution saturated with salts is cooled and thereby creates the conditions for precipitation (crystallization) of salt on the seed crystal. Data about these crystallizers have been published recently [24, 25].

In the numerical solution, methodological developments were used for solving fluid mechanics problems by finite difference and finite element methods, which are presented in the monograph [27] and implemented in the CrystmoNet software package [26]. For implementation, they also used to the Ansys[®]/CFD licensed programs, information about which is available at <https://www.ansys.com/products/fluids>, and to the Cradle[®]SC/Tetra software package, the description and verification examples of which are at the link <https://www.cradle-cfd.com>.

2. General characteristics of continuous-flowing and non-flowing crystallizers

The investigated continuous-flowing crystallizer is shown in Figure 1a. It includes the following components: cylindrical plexiglass container, tubes for solution inflow and outflow, mixer with rotation mechanism and pump for solution. The solution completely fills container 1, in which the hydrodynamic flows are caused by solution inflow from tube 2 and its outflow through tube 3, as well as by the action of internal rotating mixer 4. The flow structure is also affected a crystal shape and its location 5. The crystallizer sizes are following: radius – 0.06 m, height – 0.185 m, length of crystal face - 0.01 m. The flow was visualized by using small aluminum particles (size of scaly particles about 10–15 μm). The flow structure is observed in the central meridional section using a flat, small thickness (1–2 mm) light beam. Digital photo and video cameras were used for visualization of flow structures and measurements of flow velocities.

Figure 1b shows that the reverse mixer rotation causes a complex and spatially non-uniform flows in crystallizer. The flow control for creation of “correct” hydrodynamic flow around growing crystal faces is difficult task. The mixer presence can be explained by the desire to achieve such conditions due to good salt mixing in solution. It is noticeable, that the solution is involved in an intense rotational movement in central container part. It mainly contributes to its good mixing near rotating mixer. The flow is weaker in central



Fig. 1. Functioning continuous-flowing crystallizer (a): 1 – container; 2, 3 – tubes for solution inflow and outflow; 4 – mixer; 5 – crystal; (b) visualized flow structure during mixer reversed rotation at 1.57 rad/s.

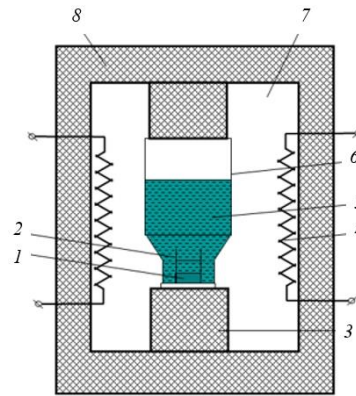


Fig. 2. Functioning non-flowing crystallizer: 1 – crystal, 2 – shape-former (glass), 3 – crystal stand, 4 – heater, 5 – solution, 6 – crystallizer wall, 7 – air, 8 – thermal insulation.

container part. It may mean a lesser effect on salt mass transfer during flow around the crystal. Although the flow near crystal is low-intensity, there is a complex spatially inhomogeneous flow structure near its surface. It means that the velocity and direction of flow around the crystallization surface change.

The disadvantage of continuous-flowing crystallizers is their design complexity due to the presence of rotation mechanisms inside the solution (elements for solution mixing etc.), which lead to the nucleation of spontaneous crystals in solution and defect formation in growing crystal.

The model of non-flowing crystallizer is shown in Figure 2. In non-flowing crystallizer, a solution stability maintains long time and prevents the formation of spontaneous crystals. However, a crystal growth is very long process, which is carried out a month with a gradual decrease in temperature by 1–7 K [24].

3. Mathematical description of hydrodynamic processes in water-salt solutions

The flow and mass transfer mathematical modeling in water-salt solutions, which are saturated at high temperature is carried out within the framework of continuous medium. Such saturated salt solution is used to crystal growth at lower temperatures in continuous-flowing and non-flowing crystallizers.

To grow KDP crystals in functioning continuous-flowing crystallizer (see Fig. 1a), the solution is salt pre-saturated in separate container at high temperature (342 K), corresponding to the high salt solution saturation — C_{eo} . Then, this saturated solution flows through connecting tube in crystallizer, in which the equilibrium salt concentration — C_e at lower working temperature (305 K) is maintained. At sufficient excess of $C_{eo} > C_e$ the salt solution supersaturation is achieved, which is necessary for crystal growth. Thermal convection is not taken into account, because the constant temperature is maintained in continuous-flowing crystallizer.

For non-flowing crystallizer (Fig. 2), the preparation of saturated solution and crystal growth are carried out in the same vessel, which is preliminarily heated strongly in order to obtain the solution with high salt concentration. Then this solution is cooled during long time due to an effective thermal insulation of working vessel. There is a volumetric salt precipitation or its deposition on solid surfaces in crystallizer. The crystalline nuclei presenting in solution grow according to thermodynamic laws, which can be taken into account with framework of mentioned continuous medium model.

3.1. Calculation of hydrodynamic processes on basis of complete Navier–Stokes equations

The solution motion is described by Navier–Stokes equations for viscous incompressible fluid with constant thermophysical properties: constant coefficients of viscosity, thermal conductivity, heat capacity, and diffusion. The density changes upon varied temperature and composition of solution is taken into account in Boussinesq approximation, which follows from Navier–Stokes equations for compressible fluid under the assumption that the fluid is dynamically and statically incompressible, that is, its density is not related to pressure, but may depend on temperature and impurity concentration. Boussinesq's approximation also takes into account of density change as functions of temperature and impurity concentration. State equation for such model is written as follows:

$$\rho = \rho(T, C),$$

where T — temperature and C — impurity concentration. It is considered that during convection a density is $\rho = \rho_o + \rho'$, where ρ_o satisfies to hydrostatics equations, and ρ' is small deviation. Then the thermal and concentration coefficients of density changes are defined as:

$$\beta_T = -\frac{1}{\rho_o} \frac{\partial \rho}{\partial T}, \quad \beta_C = -\frac{1}{\rho_o} \frac{\partial \rho}{\partial C}.$$

Navier–Stokes and continuity equations can be written in vector form [27]:

$$\frac{\partial \mathbf{V}}{\partial t} + (\mathbf{V}\nabla)\mathbf{V} = -\frac{1}{\rho_o} \nabla P + \nu \Delta \mathbf{V} + \mathbf{F}, \quad \text{div} \mathbf{V} = 0. \quad (1)$$

Here ∇ and Δ denote the gradient and Laplacian of functions, respectively. The solution temperature and impurity concentration changes during thermal convection are calculated by using the following heat and mass transfer equations:

$$\begin{aligned} \rho C_p \left(\frac{\partial T}{\partial t} + (\mathbf{V}\nabla)T \right) &= \lambda \Delta T, \\ \frac{\partial C}{\partial t} + \mathbf{V}\nabla C &= D \Delta C, \end{aligned}$$

where t — time, ρ_o — solution density, ν — kinematic viscosity, \mathbf{F} — body force (buoyancy, vibration, etc). For buoyancy forces:

$$\mathbf{F} = \mathbf{g}(\beta_T \delta T + \beta_C \delta C).$$

In a continuous-flowing crystallizers: $\mathbf{F} = \mathbf{0}$.

The desired variables in these equations are following: velocity vector \mathbf{V} , pressure P , temperature T , impurity concentration C (more precisely – their deviations from static values, which depend on spatial coordinates and time t). The model parameters are following: density ρ , kinematic viscosity $\nu = \mu/\rho$ (μ — dynamic viscosity), thermal conductivity λ , diffusion D , specific heat at constant pressure C_p , as well as gravity acceleration \mathbf{g} and coefficients of thermal and concentration density changes β_T and β_C .

The natural thermal and concentration convections are not taken into account for continuous-flowing crystallizers due to their thermostatic control and high solution pumping rate. Temperature in non-flowing thermostatic crystallizers decreases extremely slowly, so thermal convection can be taken into account in Boussinesq's approximation.

3.2. Calculation of hydrodynamic processes based on $(k - \varepsilon)$ -turbulence model

Let consider the increased sizes of crystallizer and crystal at same solution inflow rate into crystallizer. In this case Reynolds number Re increases to supercritical values ($Re \approx 10^5$), corresponding to turbulent flows. Widely studied in [29] standard $(k - \varepsilon)$ -turbulence model [28] may be applied for practical calculations. According to this model, Navier–Stokes equations are applied in averaged form. The flow variables are written as the sum of average and fluctuating components (that is $\mathbf{V} = \bar{\mathbf{V}} + \mathbf{V}'$, $P = \bar{P} + P'$ etc.).

Navier–Stokes equations (1) time averaging leads to additional terms characterizing turbulent (Reynolds) stresses. “Turbulent” viscosity in addition to Reynolds stresses is introduced in $(k - \varepsilon)$ -model, which differs from molecular viscosity μ . It characterizes a flow development, which depends on temporal history and spatial flow structure.

The equations for average values, known as the Reynolds equations, are written in component-by-component form as follows [29]:

$$\rho_o \left(\frac{\partial \bar{V}_i}{\partial t} + \bar{V}_j \frac{\partial \bar{V}_i}{\partial x_j} \right) = \frac{\partial}{\partial x_j} \left(\bar{\sigma}_{ij} - \rho \bar{V}_i \bar{V}_j \right). \quad (2)$$

The terms $\rho \bar{V}_i \bar{V}_j$ are called as Reynolds stresses. Turbulent fluid motion is described by 4 equations including 10 unknowns: 3 velocity components, pressure, 6 Reynolds stresses.

The closure of turbulent system equations is based on various relationships between Reynolds stresses and average flow parameters. Some of them are obtained by introducing turbulent analogues, for example, the turbulent viscosity μ_t as an analogy with molecular dynamic viscosity:

$$-\rho \bar{V}_i \bar{V}_j = \mu_t \left(\frac{\partial V_i}{\partial x_j} + \frac{\partial V_j}{\partial x_i} \right).$$

The development of turbulence is analyzed by using turbulent kinetic energy k and turbulent dissipation rate ε for the calculation of which two additional semi-empirical equations are used in following form:

$$\begin{aligned} \frac{\partial(\rho k)}{\partial t} + \frac{\partial(\rho k V_i)}{\partial x_i} &= \frac{\partial}{\partial x_j} \left[\frac{\mu_t}{\sigma_k} \frac{\partial k}{\partial x_j} \right] + 2\mu_t E_{ij} E_{ij} - \rho \varepsilon, \\ \frac{\partial(\rho \varepsilon)}{\partial t} + \frac{\partial(\rho \varepsilon V_i)}{\partial x_i} &= \frac{\partial}{\partial x_j} \left[\frac{\mu_t}{\sigma_\varepsilon} \frac{\partial \varepsilon}{\partial x_j} \right] + C_{1\varepsilon} \frac{\varepsilon}{k} 2\mu_t E_{ij} E_{ij} - 2C_{2\varepsilon} \rho (k^2/\varepsilon), \end{aligned}$$

where V_i — velocity components in according directions, E_{ij} – strain rate components. There are a number of constants in these equations: $C_p = 0.09$; $\sigma_k = 1.00$; $\sigma_\varepsilon = 1.30$; $C_{1\varepsilon} = 1.44$; $C_{2\varepsilon} = 1.92$. In this case the turbulent viscosity μ_t is determined from calculated values k and ε as:

$$\mu_t = \rho C_p (k^2/\varepsilon).$$

A turbulent boundary layer on solid surfaces is modeled using “wall” function [28], which relates velocity and shear stress at grid node, which is closest to solid surface.

3.3. Mass transfer in one-component salt solution

Navier–Stokes equations are solved jointly with convective salt transfer equation are solved for KDP crystal growth:

$$\frac{\partial M}{\partial t} + \mathbf{V} \nabla M = D \Delta M,$$

where $M = \rho_o C$ is mass salt component in solution, $C = (C - C_e)/(C_{eo} - C_e)$ is relative salt mass in 1 kg of solution. The parameters of hydrodynamic model are given in Table 1, which shows equilibrium salt concentrations at 305 and 342 K, too.

Table 1. Parameters of hydrodynamic model.

Parameter	Dimension		Symbol	Value
Solution dynamic viscosity	kg/(m s)		$\mu = \nu \times \rho_o$	$1.53 \cdot 10^{-4}$
Salt diffusion coefficient	m ² /s		D	$7.5 \cdot 10^{-10}$
Solution density	kg/m ³		ρ_o	1269
Crystal density	kg/m ³		$\rho_o s$	2338

Equilibrium concentration ($T = 305$ K)	kg/(kg solution)		C_e	0.2174
Equilibrium concentration ($T = 342$ K)	kg/(kg solution)		C_{eo}	0.3422

The following boundary conditions are set for calculation of required velocity and salt concentration distributions:

The following boundary conditions are set for calculation of required velocity and salt concentration distributions:

- at solution inflow from tube - jet velocity and salt concentration;
- at solution outlet from crystallizer - flow velocity and corresponding salt flux, according to mass preservation law;
- at walls of crystallizer - zero velocity and salt flux;
- at mixer - velocity components;
- at growing crystal surface – velocity components;
- for salt transfer – mass balance relation:

$$\rho_o D \frac{\partial C}{\partial n} = R(\rho_s - C_e \rho_o),$$

where R is crystallization rate calculated using following thermodynamic formula:

$$R = \beta C_e h k T \sigma^2 / (19\alpha). \quad (3)$$

Formula (3) conjugates thermodynamic micromodel and hydrodynamic macromodel for calculation of current salt solution supersaturation near crystallization surface and for estimation of crystal growth rate on basis of parameters from Table 2. Such crystal growth rate is used at next time steps in mass balance ratio on crystal surface.

Table 2. Calculation parameters for (100) facet crystallization rate

Parameter	Dimension	Symbol	Value
Temperature	K	T	305
Boltzmann constant	J/K	k	$1.38 \cdot 10^{-23}$
Kinetic coefficient	m/s	β	$9.55 \cdot 10^{-5}$
Step specific energy	J/m ²	α	$19.5 \cdot 10^{-3}$
Step height	m	h	$7 \cdot 10^{-10}$
Initial supersaturation	–	σ_o	0.09

The salt supersaturation at the crystallization surface calculated with using calculated concentration is:

$$\sigma = (C - C_e) / C_e.$$

3.4. Mass transfer in two-component salt solution

In case of KCNSH mixed crystal growth the Navier–Stokes equations are solved jointly with two equations describing the transport of two salts:

$$\frac{\partial M_i}{\partial t} + \mathbf{V} \nabla M_i = D_i \Delta M_i \quad (i = 1, 2),$$

where $M_i = \rho_o C_i$ is salt concentrations in solution [kg/m³], ρ_o — solution density and C_i — relative salt masses per 1 kg of solution, index “ i ” corresponds to following salt numbers: 1 — KCSH; 2 — KNSH.

The authors of this article did not find literature information for diffusion coefficients of KCSH and KNSH salts in water solutions. Therefore, known values for cobalt (CoCl_2) and nickel (NiCl_2) salts were used in calculations. The difference in distribution of nickel and cobalt salt concentrations along the crystal face largely depends upon the ratio of their diffusion coefficients. Since in these compounds, as well as in KCSH and KNSH, the difference in diffusion coefficients is determined by different mobilities of Co^{2+} and Ni^{2+} ions, it can be assumed that the values of diffusion coefficients in both cases will be close. Table 3 contains additional parameters for the mixed crystal growth model involved in calculations.

Table 3. Additional parameters of hydrodynamic model for mixed crystal

Parameter	Dimension	Symbol	Value
Diffusion coefficient of 1-st salt	m^2/s	D_1	$1.217 \cdot 10^{-9}$
Diffusion coefficient of 2-nd salt	m^2/s	D_2	$1.075 \cdot 10^{-9}$
Solution density	kg/m^3	ρ_o	1115
Crystal density	kg/m^3	C_{el}	2240
Equilibrium concentration of 1-st salt ($T = 316 \text{ K}$)	$\text{kg}/(\text{kg of solution})$	C_{e1}	0.044
Equilibrium concentration of 2-nd salt (342 K)	$\text{kg}/(\text{kg of solution})$	C_{e2}	0.089

In contrast to one-component solution, the mass balance ratio on the crystal surface is written for each salt:

$$\rho_{oi} D \frac{\partial C_i}{\partial n} = R(C_{si} \rho_s - C_{ei} \rho_o) \quad (i = 1, 2).$$

The values C_{si} take into account of distribution coefficient measured for these salts.

It relates the concentrations in crystal and solution:

$$K = C_{s2} C_1 / (C_{s1} C_2) = 3.7,$$

where $C_{s1} + C_{s2} = 1$. As a result, the required formulas for C_{si} calculation take the form:

$$C_{s1} = C_1 / (C_1 + KC_2), \quad C_{s2} = KC_2 / (C_1 + KC_2),$$

where C_i — salt concentrations in solution on the boundary of phases, which are determined during time iterations.

Table 4. Calculation parameters for KCNSH crystal growth rate.

Parameter	Dimension	Symbol	Value
Temperature	K	T	316
Kinetic coefficient	m/s	β	$5 \cdot 10^{-4}$
Specific energy of (110) step	J/m^2	α	$19.5 \cdot 10^{-3}$
Height of (110) step	m	h	$5.3 \cdot 10^{-10}$
Initial supersaturation	—	σ_o	0.09

The crystallization rate for both salts is calculated by formula (3) taking into account of crystallographic parameters given in Table 4.

Their supersaturation at crystallization surface is calculated, according to the data for salt concentrations:

$$\sigma_i = (C_i - C_{ei}) / C_{ei} \quad (i = 1, 2) \quad (5)$$

4. Hydrodynamics and mass transfer in continuous-flowing crystallizers

The continuous-flowing crystallizers are thermostatic at set temperature, which is lower the saturation temperature for creation of required solution supersaturation. The flow in such crystallizers is depending on sizes and allocation of holes, velocities and directions of solution inflow and outflow; rates and directions of mixer rotation. The crystal growth largely depends upon a flow around the crystal and salt flux on its surface. Also, the solution state affects on crystal growth by means of salt composition purity, its salt saturation and temperature. These factors are the main subject of technological research and fairly well controlled during a solution preparation and crystal growth process.

4.1. Results of mathematical modeling the functioning KDP crystallizer with 3D solution inflow

The calculation model scheme of functioning continuous-flowing crystallizer (see Section 2) is shown in Figure 3a.

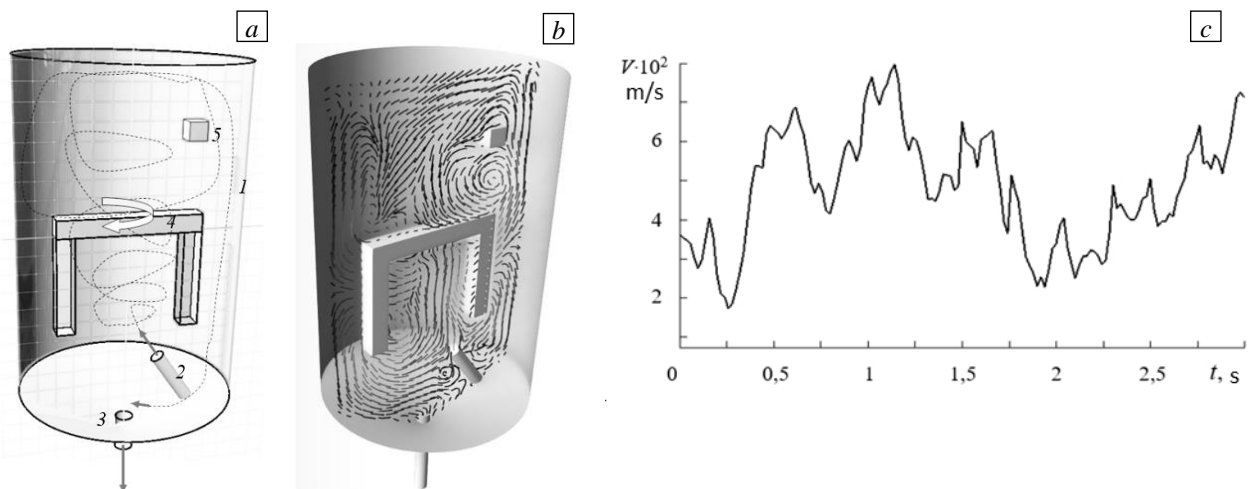


Fig. 3. Calculation scheme of functioning crystallizer (a); flow structure in meridional cross-section (b); velocity modulus oscillations nearly crystal surface (c). Here on scheme (a) the following designations are accepted: 1 – container; 2, 3 – tubes for solution inflow and outflow; 4 – mixer (circular arrow-tape shows its rotation direction relatively to container axis); 5 – crystal model; dotted line schematically shows incoming jet trajectory during mixer rotation.

The solution completely fills container 1, in which hydrodynamic flows are caused by solution inflow from tube 2 and its outflow through tube 3, as well as by rotation of internal mixer 4. In addition, the flow structure is dependent by shape and allocation of crystal 5. The crystallizer sizes are following: radius 0.06 m, height 0.185 m. The crystal has cube form with a face length 0.01 m. The solution is pumping through tube 2 at velocity $V_{in} = 0.625$ m/s. The flow direction periodically is changing during accelerated–decelerated rotation of mixer (acceleration in positive direction at +9 rad/s, its stop during 2 s, then acceleration in negative direction at –9 rad/s).

The calculations were carried out on the basis of nonstationary Navier–Stokes equations (1). The instantaneous pattern of vector lines in Figure 3b demonstrates that in central container part a solution is involved in intense vortex motion, which mainly contributes to its good mixing near rotating mixer. Far from mixer, the secondary vortices are arising, which affecting on mass salt transfer in crystal vicinity. The velocity modulus fluctuations recorded nearly to crystal surface are shown in Fig. 3c. They testify about oscillatory regime of flow around the crystal, which causes an oscillatory salt mass transfer on crystal surface. That confirms existence of non-steady vortex flow in functioning crystallizer during physical simulation (see Fig. 1b).

Additionally, the flow velocity and salt concentration were calculated during mathematical modeling. It was established that the periodic transformation of vortex flow structure and better salt solution mixing occurs. The volumetric inhomogeneity of salt concentration decreases in crystallizer. At the same time, a change of solution flow direction nearly solution/crystal interface is undesirable, because it supports crystallographic instability during crystal growth.

4.2. Results of mathematical modeling for the modernized KDP crystallizer with axisymmetric solution inflow

The modernized axisymmetric design of KDP crystallizer for formation of directed flow during crystal growth was proposed [1]. This design provides the solution flow direction and velocity controlling during its flowing around the growing crystal by using the directed and rotated flows, which corresponds to theoretical requirements of layer-by-layer crystallization. The crystal shape and placement affect on the flow structure, too.

The characteristics along crystal generatrix (crystallographic face) are interesting in such problems. In particular, the hydrodynamics and salt supersaturation knowledge for particular crystallographic facet are important for its growth rate increasing. Information about solution flow in modernized crystallizer is given in Figure 4a. The solution completely fills container 1, in which hydrodynamic flows are caused by solution inflow from tube 2 and its outflow through bottom hole 3, as well as by internal rotating mixer 4 action. The crystal 5 is fixed on an umbrella-shaped holder. The crystal and the mixer can rotate in same/opposite directions at the constant or accelerated-decelerated angular velocities Ω_C and Ω_M respectively. The crystallizer and crystal have the following sizes: $D = 0.12$ m, $H = 0.185$ m – diameter and height of cylindrical crystallizer; $d = 0.01$ m and length $h = 0.015$ m of the crystal.

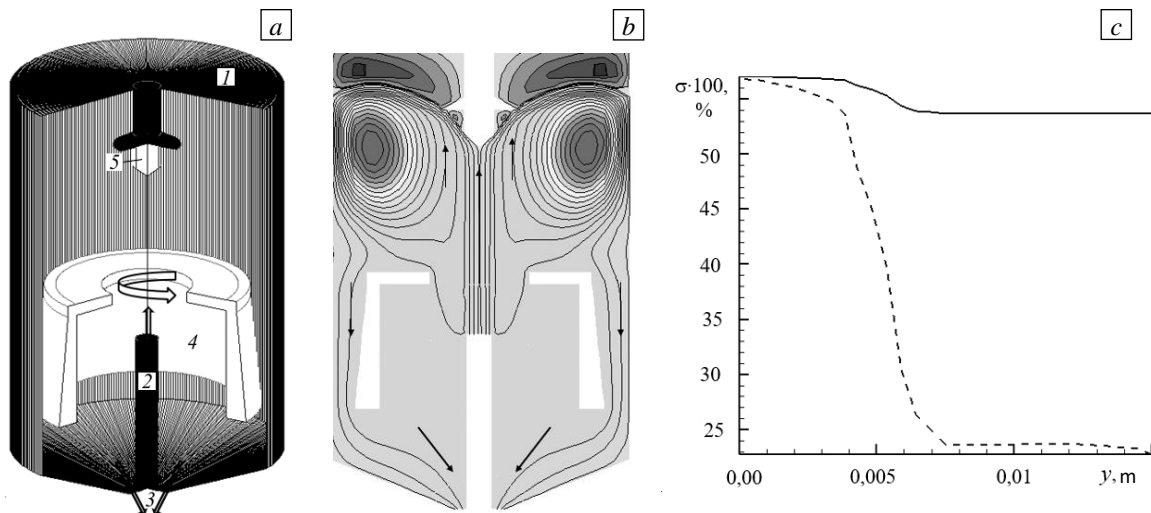


Fig. 4. Scheme of modernized KDP crystallizer (a): 1 – container; 2 – solution inflow tube and 3 – outflow hole; 4 – mixer (circular arrow shows the direction of its rotation relatively to container vertical axis); 5 – crystal; streamlines (b); supersaturation distribution (c) along the crystal surface length y (solid line) at $V_{in} = 0.6$ m/s, $\Omega_M = -1$ rad/s, $\Omega_C = 0.5$ rad/s (for comparison, the dotted line shows supersaturation at lower inflow rates ($V_{in} = 0.3$ m/s) and mixer rotation ($\Omega_M = -4$ rad/s)).

The calculations were carried out on the basis of nonstationary Navier–Stokes equations (1). The characteristic structure of solution flow is shown in Figure 4b. In addition to the directed flow from the tube, the growing crystal is affected by mixer and crystal rotations. The solution inflows from the tube at velocity $V_{in} = 0.6$ m/s, its smooth flows around the crystal conical part and forms the main vortex flow at a cone angle. However, the junction of conical and cylindrical crystal parts causes the secondary vortex formation. At mixer rotation rate $\Omega_M = -1$ rad/s and additional crystal rotation in the opposite direction at rate $\Omega_C = 0.5$ rad/s, the strong directed flow becomes even more intense due to crystal rotation. The result of hydrodynamic influence on growing crystal surface supersaturation can be seen in Figure 4c, which shows the percentage salt supersaturation on crystal conical part calculated by formula (4).

It can be seen that over the entire crystal conical part, the supersaturation level is practically the same as in solution jet impinging on it. However, the supersaturation level on cylindrical part is different: low supersaturation ($\sim 24\%$) corresponds to the low free flow velocity $V_{in} = 0.3$ m/s when the mixer rotates at a rate of $\Omega_M = -4$ rad/s, with a significant increase up to $V_{in} = 0.6$ m/s at mixer rate of $\Omega_M = -1$ rad/s and when crystal rotates at rate of $\Omega_C = -0.5$ rad/s, it increases (up to $\sim 55\%$).

4.3. Results of mathematical modeling the mixed KCNSH crystal growth during the axial directing and spiral-peripheral solution inflows

It was found that for during an axial directing solution inflow at KCNSH crystal growing, the main defect is a radial inhomogeneity of its physical properties. Therefore, the two crystal growth schemes were mathematical modelled: one corresponds to the axial directing solution inflow and another - to the spiral-peripheral solution inflow (Fig. 5a). The results are shown in Figures 5 b, c. The flow and impurities transfer were calculated in a shape former, in which a solution flows in either as a central direct-flow jet or as a spiral peripheral swirl. These calculations were carried out on basis of non-stationary Navier–Stokes equations (1) at small sizes of shape former (0.04 m in height and 0.03 m in diameter), tube diameter of 0.003 m and for four inflow velocities: $V_{in} = 0.1; 0.55; 0.9; 2.0$ m/s, which corresponds to the real experimental values during KCNSH crystal growth.

The solution circulation in crystallizer at inflow rate $V_{in} = 0.9$ m/s is shown in Fig. 5b. The inflowing jet collides with a solid barrier—the crystal surface. As a result, it changes the axial flow direction to a radial one. An intense vortex circulation occurs during the centrifugal high velocity jet near crystal surface colliding with a vessel side wall. The solution rapidly flows down in central crystallizer part (flowing outside), and a weak closed circulation (blocking flow) occurs in rest peripheral part.

The spiral jet inflowing in an experimental continuous-flowing crystallizer is realized by solution inflowing in crystallizer from a tube having a diameter of 0.003 m and allocated near edge of crystallizer bottom at angle of 60 degrees to its axis. The jet flows out tangentially to a crystallizer wall in this case. The salt precipitation on crystal surface ensures its growth from top to bottom over entire vessel diameter. The “spent” solution flows out through an open bottom part.

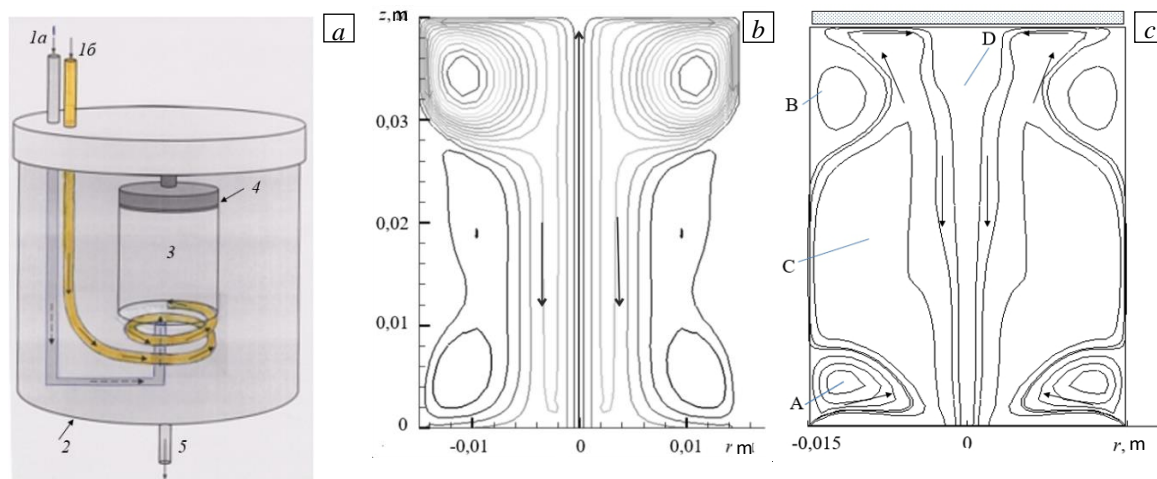


Fig. 5. Scheme of crystallizer model at central and spiral-peripheral solution inflows (a): 1a and 1b - tubes for inflow, 2 – crystallizer, 3 – shape former filled by solution, 4 – crystal, 5 – outfall tube; streamlines for central (b) and peripheral (c) solution inflowing; arrows indicate the flow direction.

The solution flow structure in meridional cross-section is shown in Figure 5c at inflow velocity $V_{in} = 0.55$ m/s. The flow caused by incoming jet rushes upwards. The meridional A and B vorticities are formed. The solution flows down through the C vortex and the central co-current D flow after flowing around the crystal. The velocity increase from 0.1 to 0.55 m/s results in A vorticity strengthening and B vorticity weakening near crystal surface. At the same time, C vorticity scale increases and region D of central direct flowing expands.

According to calculated salt concentrations, the salt supersaturation at crystal surface was found by using the formula (5). The salt supersaturation in central area of incoming jet is approximately 9% for central co-current solution inflowing (Fig. 6a). Then it monotonically is dropping to 7–8% at removal from crystal axis. The inequality of Co and Ni distribution coefficients leads to significant difference of solution supersaturation for each component.

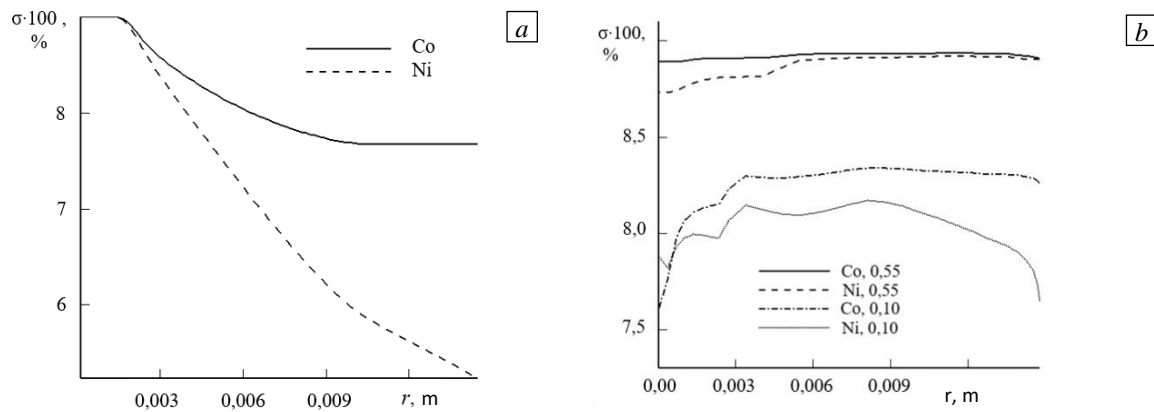


Fig. 6. Radial supersaturation profiles on the crystal surface for salt components Co and Ni in a laminar flow: at solution supersaturation in centrally flowing jet $\sigma = 9.0\%$ and inflowing velocity $V_{in} = 0.9$ m/s (a); at solution spiral-peripheral inflowing for two velocities: $V_{in} = 0.1; 0.55$ m/s (b).

Since the distribution Ni coefficient is greater than 1, and Co coefficient of Co is less than 1, the solution becomes depleted in nickel more than in cobalt, as it moves along growing face. As a result, the ratio of Co and Ni changes in solution along crystal surface. As the flow velocity increases, the number of composition variations decreases. As the solution supersaturation decreases, a crystal growth rate decreases in square proportion of supersaturation ratio (see formula (3)). As a result, the solution loses less substance along flow trajectory, and the inhomogeneity distribution of components along the crystal face decreases.

The supersaturation at crystal surface is shown in Figure 6b for two inflowing velocities ($V_{in} = 0.1; 0.55$ m/s) at spiral-peripheral solution inflowing. It can be noted that a high inflowing velocity provides a higher salt supersaturation and its better homogeneity over the entire crystal surface, which is due by an intense and uniform flowing around its surface. At the same time, the saturation value is decreasing lower for lower inflowing velocity. Moreover, its noticeable radial inhomogeneity is observed in crystal center, what is explained by the presence of more intense central vortex flowing around the crystal.

The crystallizer sizes with the spiral-peripheral solution inflowing were proportionally increased by 5 times. In this case, Reynolds number reaches the large value ($\sim 3 \times 10^4$), which corresponds to the appearance of turbulent internal flow in crystallizer. Therefore, in numerical simulation, the averaged Navier–Stokes equations (2) were solved in framework of standard ($k - \varepsilon$)-turbulence model. The calculated results showed that the high level of salt saturation on crystal surface was increased in 5 times, too. This allows to conclude that for increased size crystal growing such crystallizer design is technologically relevant today.

4.4. Accelerated-decelerated mixer rotation in crystallizer of large sizes during spiral-peripheral fluid inflowing

The application of lateral solution inflowing into crystallizer is necessary for the flow formation sufficiently densely and uniformly swirling around the crystal. It is believed that this will ensure the spatial salt flow homogeneity in growing facet direction of crystal. The effect of lateral inflowing consists in the formation of spatial swirling and complex shape flows, which may affect on crystal growth and determine temperature, flow velocity and direction, salt solution saturation.

The crystallizer design is shown in Figure 7a, in which the solution is inflowing through the side tube and flowing out through the central bottom hole. The crystal and rotating mixer are inserted into crystallizer. The crystallizer has cylindrical shape and following sizes: diameter 0.2 m, height 0.3 m. The geometrical data of other components are following: diameter of side inflowing hole is 0.01 m; diameter of central flow outlet is 0.05 m and radius of thin-walled mixer is 0.05 m. A cubic crystal with an edge length of 0.1 m is located inside the crystallizer. The required flow swirl around the crystal is achieved by corresponding spatial orientation of solution inflowing tube. The inflowing tube is oriented at 60 degrees to crystallizer lateral wall in this case.

Preliminary estimates for larger size crystallizer show the large (supercritical) Reynolds numbers corresponding to a turbulent flow. Therefore, the averaged Navier–Stokes equations (2) were numerically solved in framework of standard ($k - \varepsilon$)-turbulence model.

The flow structure analysis at lateral solution inflowing and during mixer absence (Fig. 7*b*) shows a swirling flow existence near crystal, which may be formed already at inflowing velocity of 0.06 m/s. The mixers are used usually in crystallizers. The lateral solution inflowing at rotating mixer presence is considered for comparison. The calculated results (see Fig. 7*c*) indicate that the mixer forms flows, which violate the required incoming flow swirl nearly the crystal. So, its effect is undesirable.

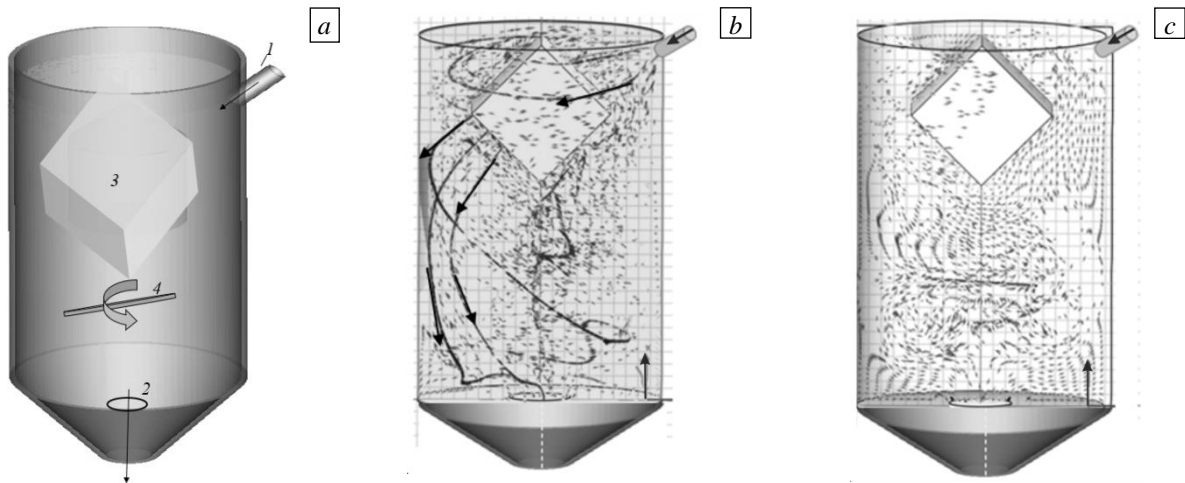


Fig. 7. Scheme of continuous-flowing crystallizer model with lateral solution inflowing (*a*): 1 – solution inflowing tube, 2 – hole on bottom for solution outflowing, 3 – crystal, 4 – rotating mixer; arrows – flow trajectories at mixer absence (*b*); visualized multi-vortex flow caused by mixer rotating at angular velocity of 5.2 rad/s (*c*).

5. Hydrodynamics and heat transfer in non-flowing crystallizers

Further, the mathematical modeling of KCNSH crystal growing from a mixture of two water-salt solutions (cobalt KCSH and nickel KNSH salts) in non-flow crystallizers is considered with according to the data [24, 25]. In them, the calculations of hydrodynamics and heat transfer were carried out on basis of Navier–Stokes equations (1) and Boussinesq’s approximation (the concentration convection was not taken into account, that is, the concentration expansion coefficient was set to zero: $\beta_c = 0$). The advantage of growth process in non-flow crystallizers consist in maintaining a solution metastability for long time and preventing the formation of spontaneous crystals. The growth of such crystals is usually carried out within a month with a gradual temperature decrease.

5.1. Calculation results for functioning non-flowing crystallizer

Scheme of mathematical modeling for functioning non-flowing crystallizer is shown in Figure 8*a* [24]. The crystal is grown in completely closed glass cylindrical container filled by solution and closed by thermal insulation, which has an air cavity and a resistive heater. At the container bottom, a cylindrical cup (a crystal shape former) is axis symmetrically mounted, inside which a crystal grows, gradually filling the cup interior.

Before growth start, a solution is saturated by salt to predetermined level at sufficiently high temperature, then a salt begins to precipitate on crystallization surface. The solution becomes depleted by released component and the crystal growth rate slows down with time, its value gradually decreases from 0.5 to 0.1 mm per day. As a result, the growth time for practically using crystals reaches 40 days. The process of crystal growth is accompanied by decreasing solution temperature, which maintains the required level of its salt saturation for an ensure of needed crystal growth rate. The needed solution temperature is maintained by heater power regulating.

The vortices structure in air gap is shown In Figure 8*a*, which affecting on hydrodynamics and temperature in salt solution. It can be noted that in vertical vortices cascade within this air gap, the most intense distinguishing vortex adjoints to the heater. Thanks to him, the main heat transfer to solution occurs from the heater. In solution itself, the main vortex arises near a side wall and secondary vortex - in vessel center. The essence of temperature distribution in the solution can be judged from Figure 8*c*. It can be seen that a high volumetric uniformity of temperature field is achieved in at solution temperature corresponding to 313.3 K. Slight vertical inhomogeneity (approximately 0.2 – 0.3 K) is observed near lower and upper ends of glass container.

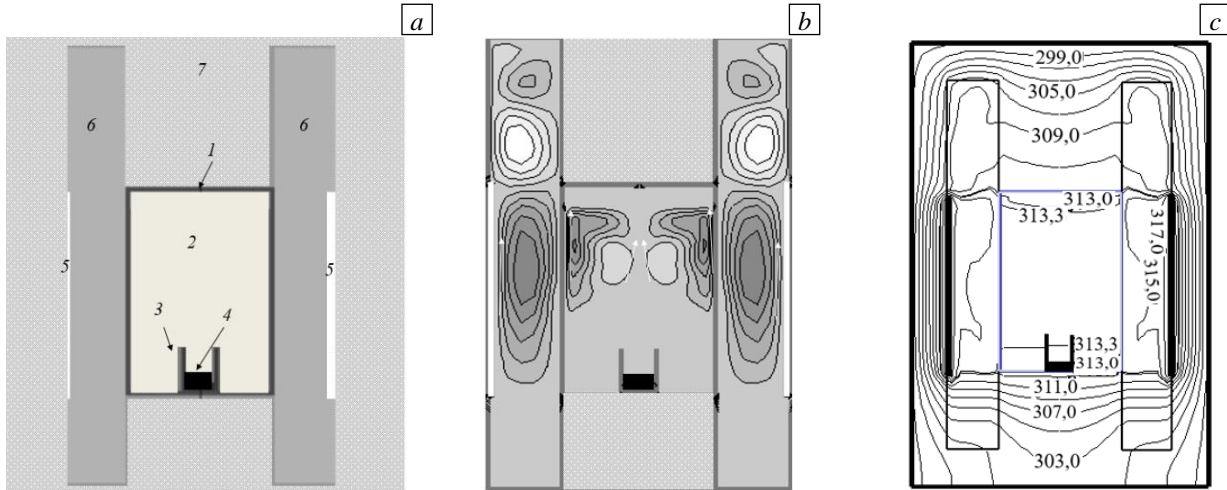


Fig. 8. Scheme of the model (a): 1 – glass cylindrical container, 2 – solution, 3 – shaper, 4 – crystal, 5 - heater, 6 - air, 7 - thermal insulation; vortices in solution 2 and in air cavity 6, arrows show the direction of flow (b); isotherms in crystallizer (c)

5.2. Calculation results for modernized non-flowing crystallizer

The modernized non-flowing crystallizer is proposed in patent [25]. Its advantage is a location of main solution mass in upper part at temperature above the liquidus temperature (i.e., in unsaturated state) and in lower solution part at temperature below the liquidus temperature (i.e., in growth state with much smaller volume). It makes possible significantly (almost in 100 times) to reduce the solution volume in supersaturated state. The presence of two independent heaters provides the supersaturated solution state in growing part and the unsaturated solution state in upper crystallizer part during entire growth process.

The scheme of mathematical model for such modernized crystallizer is shown in Figure 9a. The corresponding distribution of isotherms and the graph of axial temperature distribution are shown in Figures 9b and 9c. It is possible to select the zone 1 with a practically constant temperature of 314–314.5 K and the zone 2 with a sharp decrease in temperature from 314 to 309.5 K. This confirms the correctness of modernized crystallizer design, which creates cooling conditions in glass container neck corresponding to the required crystallization conditions.

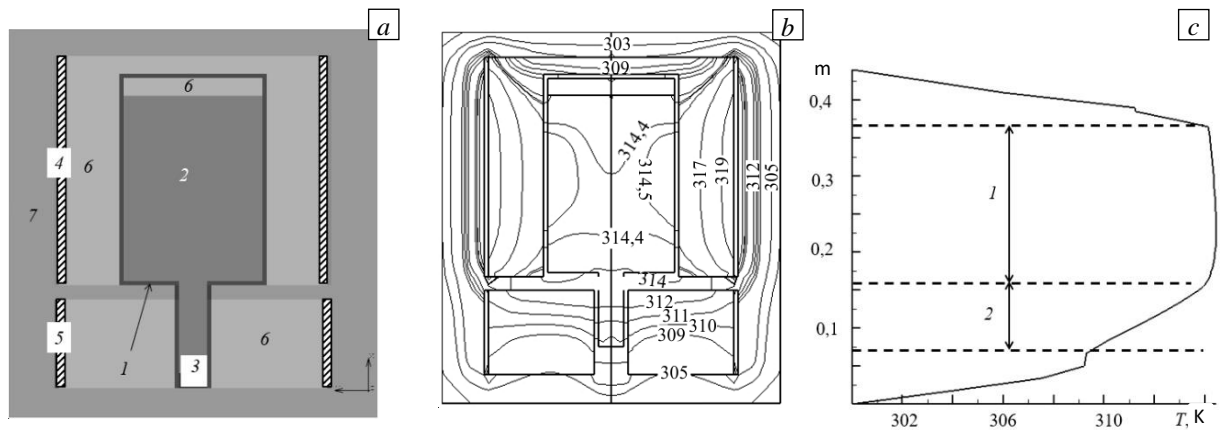


Fig. 9. Scheme of modernized crystallizer model (a): 1 – glass container, 2 – solution, 3 – crystal, 4 – upper heater, 5 – lower heater, 6 – air, 7 – thermal insulation; isotherms in non-flowing crystallizer (b); vertical temperature distribution on crystallizer axis (c)

The comparisons of isotherm distributions considered in this section for two non-flowing crystallizers allow to conclude that the modernized crystallizer in greater extent avoids a parasitic spontaneous crystallization due to its more correct shape.

6. Conclusion

The present review article characterizes the current state of researches in hydromechanics of growing technically valuable KDP and KCNSH crystals from water–salt solutions.

The referred works on physical modeling with using aluminum powder for flow visualization showed too complex flow picture in functioning continuous-flowing crystallizers due to the presence of various design mixers, three-dimensional solution inflow and outflow and crystal placing. Physical modeling turned out ineffectively for establishment of quantitative data about the solution salt saturation, which play a decisive role in understanding the crystallization processes. Therefore, for growth of these crystals in continuous-flowing and non-flowing crystallizers the main attention is paid to a development of mathematical models of these growing processes. For laminar regimes, the models based on the complete Navier–Stokes equations are used together with the equations of impurity and heat transfer in the Boussinesq’s approximation. For turbulent regimes, the flow velocities are calculated on the basis of the standard $(k - \varepsilon)$ -turbulence model.

With using the modern software, the spatial flows and salt components concentration distributions were studied in various crystallizers (both functioning and proposed for implementation in technological practice). New design is proposed for an axisymmetric continuous-flowing crystallizer, providing a high salt saturation near KDP crystal growing surface. It was established that the effects of axial salt segregation are significantly manifested at low (less than 0.1 m/s) flow velocities around the crystal. However, such velocities are not technologically significant, because important practical results correspond to crystal flow velocities greater than 0.5 m/s.

It has been shown that a spiral peripheral solution inflow to growing KCNSH crystal significantly reduces an undesirable radial inhomogeneity of its properties in comparison of crystal growing with direct central solution inflow into crystallizer. Mathematical modeling made possible an analysis of thermal fields in functioning and modernized non-flowing crystallizers. The assumption of the inventors of the modernized non-flowing crystallizer about the existence of two thermal zones (in the main volume and in the neck), which provides a more stable process of KCNSH crystal growth, was quantitatively confirmed.

In general, it can be noted that there are still problematic issues related to the interface of micromodels of crystallization with the data of hydromechanical macromodelling, which are discussed in Section 1 and which should be addressed in the future.

Acknowledgments. The present work was supported by the Ministry of Science and Higher Education within the framework of the Russian State Assignment under contract No. AAAA-A20-120011690136-2.

References

1. Voloshin A.E., Rudneva E.B., Manomenova V.L. Forming features of inhomogeneity of the crystals grown from solutions. *Vestnik RFFI*, 2014, vol. 82, no. 2, pp. 29-33.
2. Booth N.A., Chernov A.A., Vekilov P.G. Characteristic length scales of step bunching in KDP crystal growth: in situ differential phase-shifting interferometry study. *J. Cryst. Growth*, 2002, vol. 237-239, pp. 1818-1824. [https://doi.org/10.1016/S0022-0248\(01\)02101-7](https://doi.org/10.1016/S0022-0248(01)02101-7)
3. Chernov A.A. Step bunching and solution flow. *J. Optoelectron. Adv. Mater.*, 2003, vol. 5, no. 3, pp. 575-587. https://joam.inoe.ro/arhiva/pdf5_3/Chernov.pdf
4. Vekilov P.G., Alexander J.I.D., Rosenberger F. Nonlinear response of layer growth dynamics in the mixed kinetics-bulk transport regime. *Phys. Rev. E*, 1996, vol. 54, pp. 6650-6660. <https://doi.org/10.1103/PhysRevE.54.6650>
5. Smolsky I.L., Zaitseva N.P., Rudneva E.B., Bogatyreva S.V. Formation of “hair” inclusions in rapidly grown potassium dihydrogen phosphate crystals. *J. Cryst. Growth*, 1996, vol. 166, pp. 228-233. [https://doi.org/10.1016/0022-0248\(96\)00080-2](https://doi.org/10.1016/0022-0248(96)00080-2)
6. Coriell S.R., Murray B.T., Chernov A.A., McFadden G.B. Step bunching on a vicinal face of a crystal growing in a flowing solution. *J. Cryst. Growth*, 1996, vol. 169, pp. 773-785. [https://doi.org/10.1016/S0022-0248\(96\)00470-8](https://doi.org/10.1016/S0022-0248(96)00470-8)
7. Coriell S.R., Murray B.T., Chernov A.A., McFadden G.B. The effect of a shear flow on the morphological stability of a vicinal face: Growth from a supersaturated solution. *Adv. Space Res.*, 1998, vol. 22, pp. 1153-1158. [https://doi.org/10.1016/S0273-1177\(98\)00158-6](https://doi.org/10.1016/S0273-1177(98)00158-6)

8. Dinakaran S., Verma S., Das S.J., Kar S., Bartwal K.S. Influence of forced convection on unidirectional growth of crystals. *Phys. B: Condens. Matter*, 2010, vol. 405, pp. 3919-3923. <https://doi.org/10.1016/j.physb.2010.06.028>
9. Robey H.F., Potapenko S.Y. Ex situ microscopic observation of the lateral instability of macrosteps on the surfaces of rapidly grown KH_2PO_4 crystals. *J. Cryst. Growth*, 2000, vol. 213, pp. 355-367. [https://doi.org/10.1016/S0022-0248\(00\)00025-7](https://doi.org/10.1016/S0022-0248(00)00025-7)
10. Vartak B., Yeckel A., Derby J.J. Time-dependent, three-dimensional flow and mass transport during solution growth of potassium titanyl phosphate. *J. Cryst. Growth*, 2005, vol. 281, pp. 391-406. <https://doi.org/10.1016/j.jcrysgro.2005.04.037>
11. Chernov A.A., Rashkovich L.N., Vekilov P.G. Steps in solution growth: dynamics of kinks, bunching and turbulence. *J. Cryst. Growth*, 2005, vol. 275, pp. 1-18. <https://doi.org/10.1016/j.jcrysgro.2004.10.094>
12. Zhou C., Li M., Yin H., Hu Z., Yin H., Wang B., Cuiet O. Simulation of the flow and mass transfer for KDP crystals undergoing 2D translation during growth. *J. Cryst. Growth*, 2016, vol. 450, pp. 103-118. <https://doi.org/10.1016/j.jcrysgro.2016.05.052>
13. Liu H., Li M., Zhu Y. An analysis of flow and mass transfer of solution growth of $\text{NH}_4\text{H}_2\text{PO}_4$ crystals by the modified eed mounting geometries. *J. Cryst. Growth*, 2020, vol. 545, pp. 125729. <https://doi.org/10.1016/j.jcrysgro.2020.125729>
14. Masalov V.M., Vasilyeva N.A., Manomenova V.L., Zhokhov A.A., Rudneva E.B., Voloshin A.E., Emelchenko G.A. Growth of mixed $\text{K}_2(\text{Ni},\text{Co})(\text{SO}_4)_2 \cdot 6\text{H}_2\text{O}$ crystals under stationary conditions of supercooling and forced convection of the aqueous solution. *J. Cryst. Growth*, 2017, vol. 475, pp. 21-25. <https://doi.org/10.1016/j.jcrysgro.2017.05.028>
15. Voloshin A.E., Manomenova V.L., Rudneva E.B., Vasilyeva N.A., Masalov V.M., Zhokhov A.A., Emelchenko G.A. Growth of high-perfect mixed $\text{K}_2\text{Ni}_x\text{Co}_{1-x}(\text{SO}_4)_2 \cdot 6\text{H}_2\text{O}$ crystals for fabrication of high-efficiency UV optical filters. *J. Cryst. Growth*, 2018, vol. 500, pp. 98-103. <https://doi.org/10.1016/j.jcrysgro.2018.08.018>
16. Vasilyeva N.A., Rudneva E.B., Manomenova V.L., Grigoriev Yu.V., Masalov V.M., Zhokhov A.A., Emelchenko G.A., Voloshin A.E. Study of the radial heterogeneity and mosaic microheterogeneity in KCNSH mixed crystals. *Crystallogr. Rep.*, 2019, vol. 64, pp. 828-833. <https://doi.org/10.1134/S1063774519050237>
17. Grigoryeva M.S., Vasilyeva N.A., Artemov V.V., Voloshin A.E. Mosaic microinhomogeneity in crystals of $(\text{Co},\text{Ni})\text{K}_2(\text{SO}_4)_2 \cdot 6\text{H}_2\text{O}$ solid solutions. *Crystallogr. Rep.*, 2014, vol. 59, pp. 276-283. <https://doi.org/10.1134/S1063774514020102>
18. Glikin A.E., Kovalev S.I., Rudneva E.B., Kryuchkova L.Yu., Voloshin A.E. Phenomena and mechanisms of mixed crystal formation in solutions. I. General concept on the example of the system $\text{KHC}_8\text{H}_4\text{O}_4\text{-RbHC}_8\text{H}_4\text{O}_4\text{-H}_2\text{O}$. *J. Cryst. Growth*, 2003, vol. 255, pp. 150-162. [https://doi.org/10.1016/S0022-0248\(03\)01189-8](https://doi.org/10.1016/S0022-0248(03)01189-8)
19. Voloshin A.E., Kovalev S.I., Rudneva E.B., Glikin A.E. Phenomena and mechanisms of mixed crystal formation in solutions. II. Mechanism of interface processes. *J. Cryst. Growth*, 2004, vol. 261, pp. 105-117. <https://doi.org/10.1016/j.jcrysgro.2003.09.025>
20. Verezub N.A., Voloshin A.E., Manomenova V.L., Prostomolotov A.I. Hydrodynamics of solution for the rapid growth of KDP crystals. *Crystallogr. Rep.*, 2018, vol. 63, pp. 280-283. <https://doi.org/10.1134/S106377451802030X>
21. Verezub N.A., Voloshin A.E., Prostomolotov A.I. Hydrodynamics and mass transfer during growth of mixed crystals from solution. *Crystallogr. Rep.*, 2019, vol. 64, pp. 979-983. <https://doi.org/10.1134/S1063774519060257>
22. Verezub N.A., Voloshin A.E., Manomenova V.L., Prostomolotov A.I. Modeling of hydrodynamics and mass transfer processes in KDP crystal growth. *Crystallogr. Rep.*, 2020, vol. 65, pp. 641-646. <https://doi.org/10.1134/S1063774520040239>
23. Prostomolotov A.I., Verezub N.A., Vasilyeva N.A., Voloshin A.E. Hydrodynamics and mass transfer during the solution growth of the $\text{K}_2(\text{Co},\text{Ni})(\text{SO}_4)_2 \cdot 6\text{H}_2\text{O}$ mixed crystals in the shapers. *Crystals*, 2020, vol. 10, pp. 982-994. <https://doi.org/10.3390/cryst10110982>
24. Zhokhov A.A., Masalov V.M., Rudneva E.B., Manomenova V.L., Vasilyeva N.A., Sukhinina N.S., Voloshin A.E., Emelchenko G.A. Growth of mixed $\text{K}_2\text{Ni}_x\text{Co}_{(1-x)}(\text{SO}_4)_2 \cdot 6\text{H}_2\text{O}$ crystals for large supercooling without spontaneous crystallization in solution. *Mater. Res. Express*, 2020, vol. 7, pp. 016202. <https://doi.org/10.1088/2053-1591/ab5fa4>
25. Zhokhov A.A., Emelchenko G.A., Masalov V.M., Sukhinina N.S., Manomenova V.L., Rudneva E.B., Vasilyeva N.A., Voloshin A.E. Device for growing mixed crystals of cobalt-nickel-potassium sulphate for

- optical filters of ultraviolet range. RF Patent No. RU 2725924. Byull. Izobret., 19 February 2020. https://i.moscow/patents/RU2725924C1_20200707 (accessed 01 April 2022)
26. Prostomolotov A.I., Ilyasov H.H., Verezub N.A. CrystmoNet remote access code for Czochralski crystal growth modelling. *Science and Technology*, 2013, vol. 3, no. 2A, pp. 18-25. <http://article.sapub.org/10.5923.s.scit.201301.04.html> (accessed 01 April 2022)
27. Polezhayev V.I., Bune A.V., Verezub N.A., Glushko G.S., Gryaznov V.L., Dubovik K.G., Nikitin S.A., Prostomolotov A.I., Fedoseyev A.I., Cherkasov S.G. *Matematicheskoye modelirovaniye konvektivnogo teplomassoobmena na osnove uravneniy Nav'ye-Stoksa* [Mathematical modeling of convective heat and mass transfer based on the Navier-Stokes equations]. Moscow, Nauka, 1987. 272 p.
28. Wilcox D.C. *Turbulence modeling for CFD*. Canada, DCW Industries, 2006. 522 p.
29. Launder B.E., Spalding D.B. *Lectures in mathematical models of turbulence*. London, New York, Academic Press, 1972. 169 p.

The authors declare no conflict of interests.

The paper was submitted 08.02.2022; approved after reviewing 18.03.2022; accepted for publication 18.03.2022.